Contents lists available at ScienceDirect

Chemical Engineering Research and Design

journal homepage: www.elsevier.com/locate/cherd

Adsorption of copper by magnetic graphene oxide-supported β-cyclodextrin: Effects of pH, ionic strength, background electrolytes, and citric acid

Xin-jiang Hu[a,b], *Yun-guo Liu*[a,b,*], *Hui Wang*[a,b], *Guang-ming Zeng*[a,b], *Xi Hu*[a,b], *Yi-ming Guo*[a,b], *Ting-ting Li*[a,b], *An-wei Chen*[a,b], *Lu-hua Jiang*[a,b], *Fang-ying Guo*[a,b]

[a] *College of Environmental Science and Engineering, Hunan University, Changsha 410082, PR China*
[b] *Key Laboratory of Environmental Biology and Pollution Control (Hunan University), Ministry of Education, Changsha 410082, PR China*

A B S T R A C T

Elucidating the influence mechanism of surrounding environmental conditions on the adsorption process is essential in application of adsorption method for heavy metal removal from wastewater. In the present work, the magnetic graphene oxide-supported β-cyclodextrin (MGO/β-CD) was synthesized and characterized by FESEM, TEM, TG–DSC, FT-IR, and zeta potential. The effects of pH, ionic strength, background electrolytes, and citric acid on the adsorption behavior of Cu(II) by MGO/β-CD were investigated. The results showed that Cu(II) adsorption was strongly dependent on solution pH and could be affected by ionic strength, background electrolytes and citric acid. The Cu(II) adsorption was increased as the $NaNO_3$ concentration increased from 0 to 0.1 M at pH < 8. The presence of $LiNO_3$, $NaNO_3$, KNO_3, NaCl, and $NaClO_4$ enhanced the Cu(II) removal slightly. The Cu(II) adsorption was also improved by citric acid. Adsorption kinetics of Cu(II) was found to follow pseudo-second-order rate equation, and the adsorption rate was controlled by film diffusion. The adsorption data showed good correlation with the Freundlich and Temkin isotherm models. The results of this work are of great significance for the application of MGO/β-CD as a promising adsorbent material for Cu(II) removal from aqueous solution.

Keywords: Copper; Magnetic graphene oxide-supported β-cyclodextrin; Ionic strength; Background electrolytes; Citric acid; Influence mechanism

1. Introduction

Adsorption is a relatively new and economical process that has proven to be very promising in the removal of contaminants from wastewater (Boudrahem et al., 2011). It is well known that adsorption of heavy metals onto adsorbents can be affected by the surrounding environmental conditions, such as pH, background electrolyte composition, and ionic strength (El-Bayaa et al., 2009; Hu et al., 2011; Liu et al., 2011). The solution pH affects the speciation of adsorbate and the surface charge of adsorbent, which may result in varying adsorption efficiency (Nomanbhay and Palanisamy, 2005). Besides, the wastewaters usually have wide ranges of pH values. Therefore, the pH of the aqueous solution plays a significant role in the wastewater treatment process (Khaled et al., 2009). What's more, in natural water or wastewater systems, several types of background electrolyte ions are present over a wide range of concentration depending on the source and the quality of the water (Boudrahem et al., 2011). The background cations in the solution may compete with heavy metal ions for available

* *Corresponding author at*: College of Environmental Science and Engineering, Hunan University, Changsha 410082, PR China. Tel.: +86 731 88649208; fax: +86 731 88822829.
E-mail address: hnuese@126.com (Y.-g. Liu).

Available online 7 June 2014
http://dx.doi.org/10.1016/j.cherd.2014.06.002
0263-8762/

adsorption sites, while the anions of background electrolytes may form water-soluble metal-anion complexes or precipitates with metal ions, thereby influencing the removal of heavy metal ions (Yang et al., 2012). Many researchers have investigated the effects of background electrolyte and ionic strength on heavy metals adsorption, and they found that the background electrolyte and ionic strength have different effects (no impact, improvement, and reduction) on the heavy metals adsorption depending on the adsorption system and solution condition (El-Bayaa et al., 2009; Jiang et al., 2010; Lam et al., 2008; Tan et al., 2007; Tao et al., 2004; Yang et al., 2006, 2012). Although these studies have given some insights into the effects of surrounding environmental conditions on heavy metals adsorption, more research is still needed in order to have a better elucidating of the influence mechanism.

As is known to all, heavy metal wastewaters contain not only metal ions but also various concentrations of organic substances, and the organic substances can react with metal ions and adsorbents, thereby influencing the removal of metal ions (Li et al., 2012). Cu and its compounds are widely used in many industries, such as electrical, electroplating, paper manufacturing, pesticides, herbicides and tannery industries (Manzoor et al., 2013). Citric acid, which is widely used in medicine, daily chemical, and food industries, is a weak organic acid with the formula $C_6H_8O_7$, and it is frequently found in industrial effluents and surface water due to its disposal. There is a high possibility that citric acid and Cu(II) ions co-exist in mixed contaminant systems. Citric acid consists of three carboxyl (—COOH) groups, which can form complexes with Cu(II) ions and interact with the groups on the adsorbent surfaces. Therefore, the presence of citric acid in the wastewater may affect the Cu(II) ions adsorption. To date, the removal of Cu(II) by various adsorbents has been studied well (Hu et al., 2013; Li et al., 2012; Parida et al., 2012). However, reports regarding the influence of citric acid on Cu(II) adsorption are scant.

Many organic and inorganic materials, such as chitosan (Hu et al., 2011) β-cyclodextrin (β-CD) (Kozlowski et al., 2005), activated carbons (Mohan and Pittman, 2006), graphene oxide (GO) (Pan et al., 2013; Zhao et al., 2011), and carbon nanotubes (Yang et al., 2011), have been applied to remove heavy metal ions from aqueous solution. GO has received world-wide attention due to its exceptional physicochemical properties (Hu et al., 2013). In a previous study, we reported a method to synthesize a magnetic graphene oxide (MGO) by coprecipitating Fe^{2+} and Fe^{3+} ions with ammonia solution in GO solution (Hu et al., 2013). This composite could be easily separated by magnetic separation from the medium. The β-CD can form inclusion complexes with various organic compounds and metal ions in its hydrophobic cavity through host–guest interaction (Chen et al., 2007; Szejtli, 1998). Therefore, graft of β-CD on the magnetic graphene oxide (MGO) surface may increase the adsorption ability of the composite for organic compounds and metal ions.

The objectives of this study were to (1) prepare and characterize magnetic graphene oxide-supported β-cyclodextrin (MGO/β-CD) and apply it as an adsorbent for Cu(II) ions removal; (2) study the influences of pH and ionic strength on Cu(II) adsorption; (3) investigate the effects of background electrolytes and citric acid on Cu(II) removal; (4) discuss the adsorption mechanism using kinetics and isotherm models.

2. Materials and methods

2.1. Materials

Graphite powder was obtained from Tianjin Hengxin Chemical Preparation Co., Ltd. β-cyclodextrin was supplied by Tianjin Guangfu Chemical Preparation Co., Ltd. $NaNO_3$, $LiNO_3$, KNO_3, and NaCl were provided by Tianjin Damao Chemical Preparation Co., Ltd. $NaClO_4$ and citric acid were purchased from Sinopharm Chemical Co., Ltd. All reagents above were of Chemical grade. The MGO was prepared by the procedure reported earlier (Hu et al., 2013). Magnetic graphene oxide-supported β-cyclodextrin (MGO/β-CD) was synthesized by grafting ethylenediamine-modified β-cyclodextrin (CD-E) onto the MGO surface using Guo's method (Guo et al., 2010).

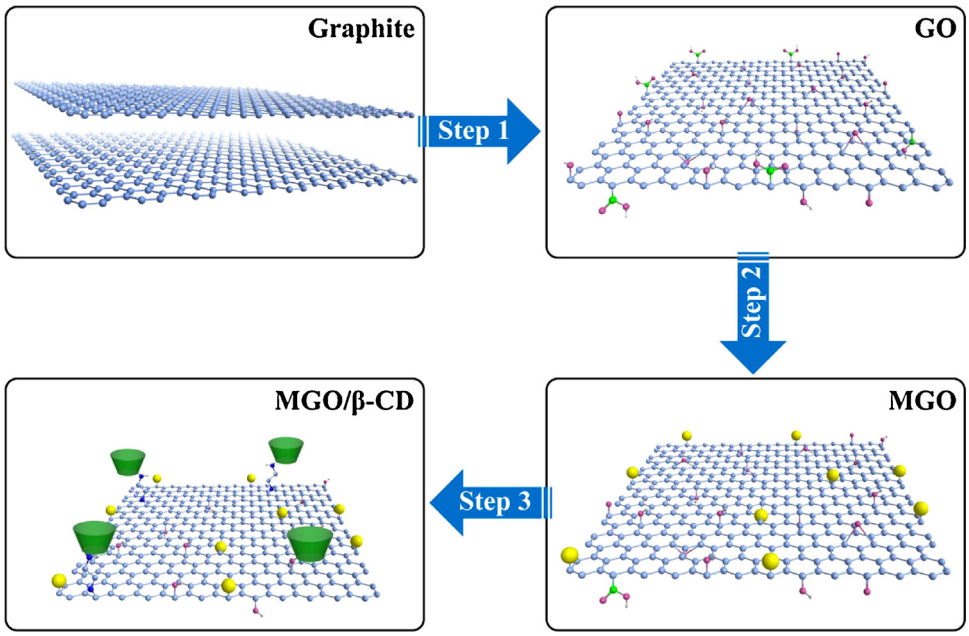

Fig. 1 – Schematic representation of the synthesis processes of MGO/β-CD from graphite: (Step1) oxidation of natural graphite to graphite oxide, followed by ultrasonication; (Step2) preparation of MGO by loading magnetic nanoparticles on the GO surface; (Step3) formation of MGO/β-CD by grafting β-CD on the MGO surface.

The CD-E was prepared according to Ohashi's work (Ohashi et al., 2006). The obtained MGO/β-CD was rinsed with ethanol and Milli-Q water until the solution was neutral and stored at room temperature. Fig. 1 shows the preparation sketch of MGO/β-CD.

2.2. Characterization

The morphology of MGO/β-CD was characterized by field-emission scanning electron microscopy (FESEM, JSM 6700F, Japan). TEM image was performed on a JEOL1230 microscope. TG and DSC curves were recorded using thermoanalytical equipment (STA 409 PC, NETZSCH, Germany). FT-IR spectrum of MGO/β-CD was measured on a spectrophotometer (Varian 3100, USA) using the KBr pellet technique. Zeta potentials were obtained by Zetasizer Nano SZ (ZEN3690, Malvern, UK).

2.3. Adsorption experiments

The stock solution (1 g/L) of Cu(II) was prepared by dissolving pure copper powder with HNO_3 solution. The solutions of different concentrations used in various experiments were obtained by diluting the stock solution. All batch adsorption experiments were performed in an incubator shaker with a shaking speed of 150 rpm. The suspension of MGO/β-CD or MGO was added to achieve the desired concentrations of different components. The pH was adjusted to desired values by adding negligible volumes of NaOH or HCl. After being mixed for 24 h, the mixture was separated by a permanent magnet. The Cu(II) concentration in the supernatant was analyzed using flame atomic absorption spectrometry (PerkinElmer AA700, USA). The quantity of Cu(II) adsorbed (q_e) was calculated using the mass balance equation (Eq. (1)).

$$q_e = \frac{(C_0 - C_e) \times V}{m} \quad (1)$$

where C_0 (mg/L) and C_e (mg/L) are the initial and final concentration of the Cu(II) solution, V (L) is the volume of the Cu(II) solution, and m (g) is the mass of MGO/β-CD or MGO.

3. Results and discussion

3.1. Characterization of MGO/β-CD

The FESEM and TEM images of MGO/β-CD are demonstrated in Fig. 2a and b, respectively. These images showed that some wrinkles were observed on the surface of MGO/β-CD and Fe_3O_4 particles were dispersed on the GO surface. The TG-DSC curves of MGO/β-CD are demonstrated in Fig. 2c. The first mass loss between 30 and 148 °C (5.9%) corresponding to the endothermic peak at 108 °C, which was attributed to the dehydration process. MGO/β-CD was found to have 59.4 wt% weight loss when the temperature range from 148 to 1000 °C, which was due to the loss of functional groups on the sheets and the degradation of grafted β-CD (Yang et al., 2009). The spectrum of MGO/β-CD (Fig. 2d) illustrated the presence of C=O in amide I (at 1657 cm^{-1}), C—N (at 1239 cm^{-1}), amide N—H (at 1576 cm^{-1}), and Fe—O in Fe_3O_4 (at 587 cm^{-1}) (Badruddoza et al., 2013; Konkena and Vasudevan, 2012). The peaks at 1028 and 942 cm^{-1} corresponded to the antisymmetric glycosidic ν_a (C—O—C) vibrations (Badruddoza et al., 2013) and the R-1,4-bond skeleton vibration of β-CD, respectively (Fan et al., 2012). As shown in Fig. 2e, the zeta potential decreased with the increase of pH and the point of zero charge (pH_{pzc}) of

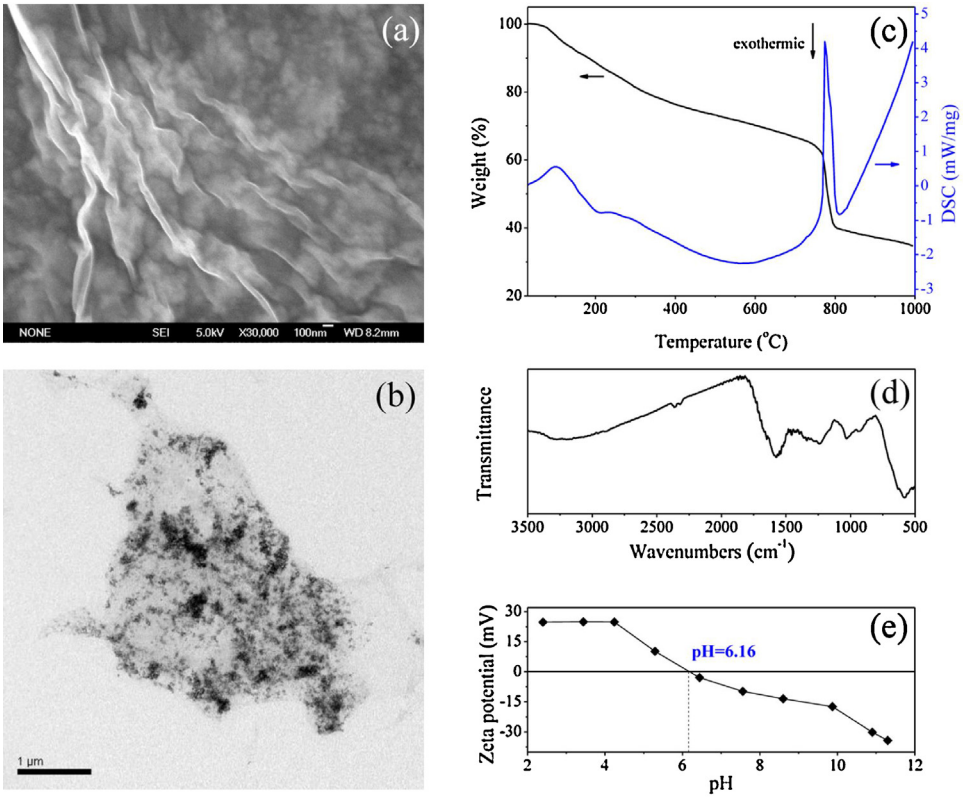

Fig. 2 – Characterization of MGO/β-CD: (a) FESEM photograph; (b) TEM photograph; (c) TG–DSC curves; (d) FT-IR spectrum; and (e) Zeta potential.

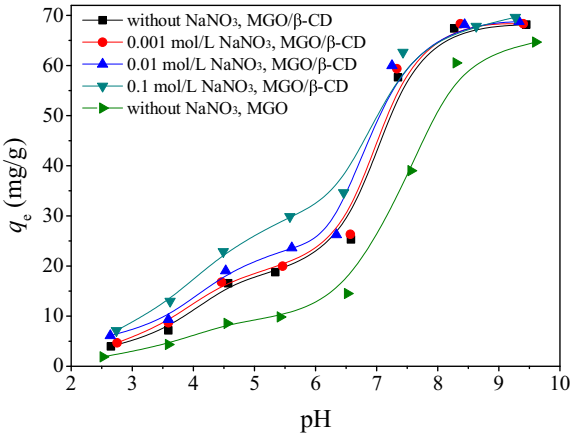

Fig. 3 – Effect of $NaNO_3$ concentration (0, 0.001, 0.01, and 0.1 mol/L) on Cu(II) adsorption onto MGO and MGO/β-CD as a function of pH: $C_{0(Cu)}$ = 10 mg/L, m/V = 0.14 g/L, T = 30 °C, t = 24 h.

MGO/β-CD was 6.16. At pH < 6.16, the zeta potentials were positive, however, the surfaces of MGO/β-CD were negatively charged at pH > 6.16.

3.2. *Effects of pH and ionic strength*

The effect of ionic strength on Cu(II) uptake as a function of pH was studied by conducting batch experiments at different concentrations of $NaNO_3$ (0, 0.001, 0.01, and 0.1 mol/L), and the obtained results are shown in Fig. 3. It can be clearly seen that the Cu(II) adsorption onto MGO/β-CD was strongly dependent on pH values. In the system without $NaNO_3$ addition, the removal of Cu(II) increased slowly with the increase of pH at pH 2.5–6, then increased quickly at pH 6–8, and at last maintained a high level at pH > 8. It is well known that the solution pH affects the speciation of Cu(II) and the surface charge of adsorbent. Relative speciation of Cu(II) as a function of pH values was calculated using the program visual MINTEQ. The results demonstrated that the predominant Cu(II) species is Cu^{2+} (>95%) at pH < 6, while the main Cu(II) species are $Cu(OH)^+$, $Cu(OH)_2(aq)$, $Cu_2(OH)_2{}^{2+}$, $Cu(OH)_3{}^-$, and $Cu_3(OH)_4{}^{2+}$ at pH > 6. At pH < 6.16, the zeta potentials were positive, thus the positive Cu^{2+} were difficult to adsorb on the positively charged surfaces of MGO/β-CD in this pH range because of the electrostatic repulsion. The surfaces of MGO/β-CD were negatively charged at pH > 6.16, therefore the positive $Cu(OH)^+$, $Cu_2(OH)_2{}^{2+}$, and $Cu_3(OH)_4{}^{2+}$ could be easily captured by the negatively charged MGO/β-CD. What's more, the Cu(II) ions could form precipitation in this pH range. Therefore, the high removal percentage at pH > 6 is mainly due to the cooperating role of precipitation of $Cu(OH)_2$ and adsorption of $Cu(OH)^+$, $Cu_2(OH)_2{}^{2+}$, and $Cu_3(OH)_4{}^{2+}$ by MGO/β-CD. Fig. 3 also shows that the Cu(II) adsorption on MGO/β-CD is higher than that on MGO at the same solid content. The hydrophobic cavity of grafted β-CD and the amino groups of grafted ethylenediamine on the MGO/β-CD surfaces can act as efficient anchors for heavy metal ions, thereby improving the adsorption capacity of MGO/β-CD (Cai et al., 2014; Da'na and Sayari, 2013; Donia et al., 2013).

From Fig. 3, we can find that the removal of Cu(II) by MGO/β-CD was affected by the concentration of the $NaNO_3$. The adsorption of Cu(II) increased as the $NaNO_3$ concentration increased from 0 to 0.1 M at pH < 8, which indicated that the Cu(II) was adsorbed as strong inner-sphere surface complexes on the surfaces of MGO/β-CD (Goldberg, 2005). The increase in $NaNO_3$ concentration reduced the electrostatic repulsion between the positively charged Cu(II) ions and the MGO/β-CD surfaces, which leaded to the increase in the number of collisions between Cu(II) ions and MGO/β-CD. The β-CD grafted on the MGO surfaces could form inclusion complexes with Cu(II) ions in its cavity through host–guest interactions, thereby resulting in the increase of Cu(II) ions adsorption as the $NaNO_3$ concentration increased. From Fig. 3, no drastic difference of Cu(II) adsorption onto the MGO/β-CD in the presence of different $NaNO_3$ concentration was observed at pH > 8, which may be due to surface precipitates at high pH values (Liu et al., 2011).

3.3. *Effect of background electrolyte ions*

To investigate the influence of background electrolyte cations on Cu(II) adsorption, the adsorption of Cu(II) on the MGO/β-CD was studied as a function of pH values in 0.01 mol/L $LiNO_3$, $NaNO_3$, and KNO_3 solutions. From Fig. 4a, the presence of $LiNO_3$, $NaNO_3$, and KNO_3 enhanced the Cu(II) removal slightly, and the effects of these background electrolytes on the Cu(II) adsorption exhibited a similar trend. Based on the above discussion, we can get that the Cu(II) ions could form inner-sphere complexes on the MGO/β-CD surfaces. However, the background electrolyte ions are usually placed in the same plane as the outer-sphere complexes (Li et al., 2012). Therefore, the effects of $LiNO_3$, $NaNO_3$, and KNO_3 on Cu(II)

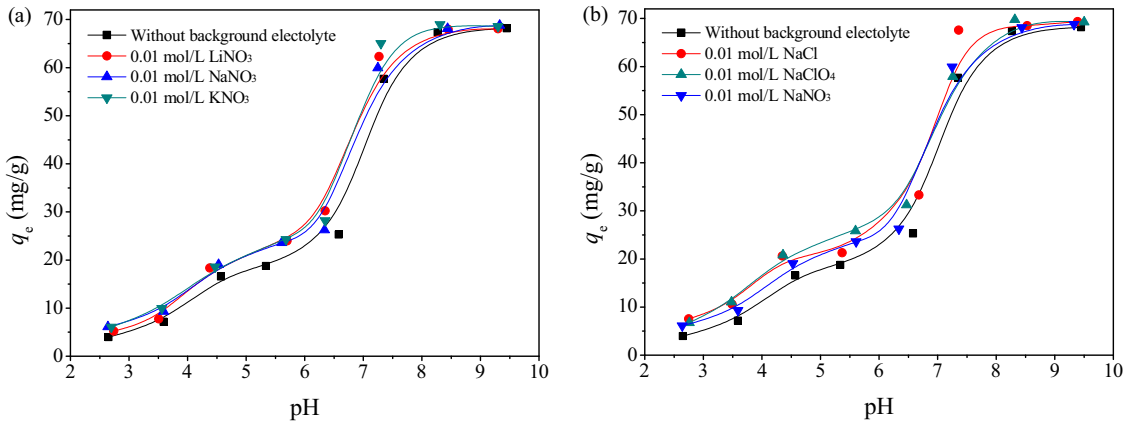

Fig. 4 – Effect of 0.01 mol/L background electrolyte cations (a) and anions (b) on Cu(II) removal by MGO/β-CD: $C_{0(Cu)}$ = 10 mg/L, m/V = 0.14 g/L, T = 30 °C, t = 24 h.

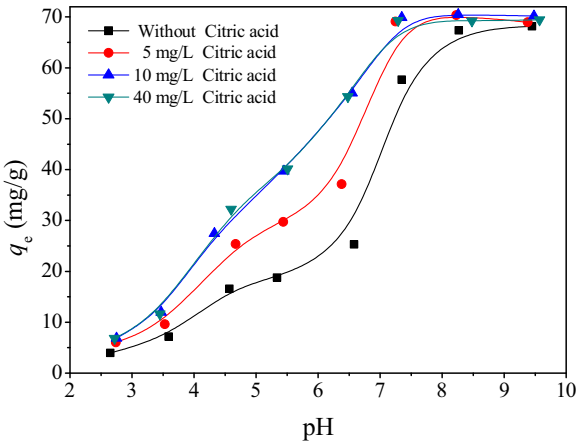

Fig. 5 – Influence of citric acid concentration (0, 5, 10, and 40 mg/L) on Cu(II) adsorption onto MGO/β-CD: $C_{0(Cu)}$ = 10 mg/L, *m*/V = 0.14 g/L, T = 30 °C, *t* = 24 h.

adsorption were not very large. The reduction of the electrostatic repulsion between the Cu(II) ions and the MGO/β-CD by the background electrolytes may be the main reason for the enhancement of the Cu(II) adsorption.

Fig. 4b shows the effect of background electrolyte anions on the adsorption of Cu(II) as a function of pH values in 0.01 mol/L NaCl, $NaClO_4$, and $NaNO_3$ solutions. The presence of NaCl, $NaClO_4$, and $NaNO_3$ in the aqueous solution improved the uptake of Cu(II) by MGO/β-CD at various pH values, and these background electrolytes had different influences on the Cu(II) adsorption under the same pH values. This phenomenon may be attributed to the different physicochemical properties of these background electrolytes.

3.4. *Effect of citric acid*

Fig. 5 shows the Cu(II) adsorption as a function of pH values in the presence of various citric acid concentrations (0, 5, 10, and 40 mg/L). As seen from Fig. 5, the presence of citric acid had significant promoting effects on the Cu(II) adsorption. This phenomenon can be explained by the complexation of surface-adsorbed citric acid and Cu(II). In the system with the presence of citric acid, the carboxyl groups (—COOH) of citric acid could interact with the groups of MGO/β-CD, and then the citric acid was adsorbed on the surfaces of MGO/β-CD. The carboxyl groups of the adsorbed citric acid could act as adsorption sites for forming complexes with Cu(II) ions. This resulted in a more favorable attraction for Cu(II) ions in the solution and enhanced the formation of MGO/β-CD-citric acid-Cu ternary surface complexes (Yang et al., 2011). From Fig. 5, we can also find that Cu(II) adsorption increased with the increase of citric acid concentration from 0 to 10 mg/L and the effects of 10 and 40 mg/L citric acid on the Cu(II) removal were very similar. The increase of Cu(II) adsorption at $C_{citric\ acid}$ < 10 mg/L is attributed to the increase in complexation of Cu(II) ions with adsorbed citric acid on MGO/β-CD surfaces. As the citric acid concentration increased from 10 to 40 mg/L, no distinct difference of Cu(II) adsorption was observed, which may be due to that the MGO/β-CD had reached saturation and could not further adsorb any citric acid and Cu(II) ions (Saman et al., 2014).

3.5. *Adsorption kinetics*

The adsorption behavior of *Cu(II)* by MGO/β-CD in relation to contact time was carried out at pH 5.5 by varying the treatment times from 0 to 24 h. The effects of 0.01 mol/L $NaNO_3$ and 10 mg/L citric acid on the *Cu(II)* adsorption were also investigated. It is noteworthy in Fig. 6a that the adsorption rate of Cu(II) uptake was very fast and the maximum uptake was observed within 10–30 min. Such a fast adsorption rate can be attributed to the absence of internal diffusion resistance and the good solubility of the MGO/β-CD (Zhang et al., 2011). The presence of 0.01 mol/L $NaNO_3$ slightly enhanced the *Cu(II)* uptake, and the citric acid significantly improved the *Cu(II)* adsorption.

To investigate the mechanism of adsorption and its potential rate-controlling steps that include mass transport and chemical reaction processes, kinetic models were exploited to analyze the experimental data (Hu et al., 2011). The non-linearized equations of pseudo-first-order (Chen et al., 2008) and pseudo-second-order (Ho et al., 1996) models can be described as follows:

$$\text{pseudo-first-order model}: \quad q_t = q_{e,1}(1 - e^{-k_1 t}) \tag{2}$$

$$\text{pseudo-second-order model}: \quad q_t = \frac{q_{e,2}^2 k_2 t}{1 + q_{e,2} k_2 t} \tag{3}$$

where q_t (mg/g) is the amount of Cu(II) adsorbed per unit mass of the MGO/β-CD at time *t* (min); $q_{e,1}$ and $q_{e,2}$ (mg/g)

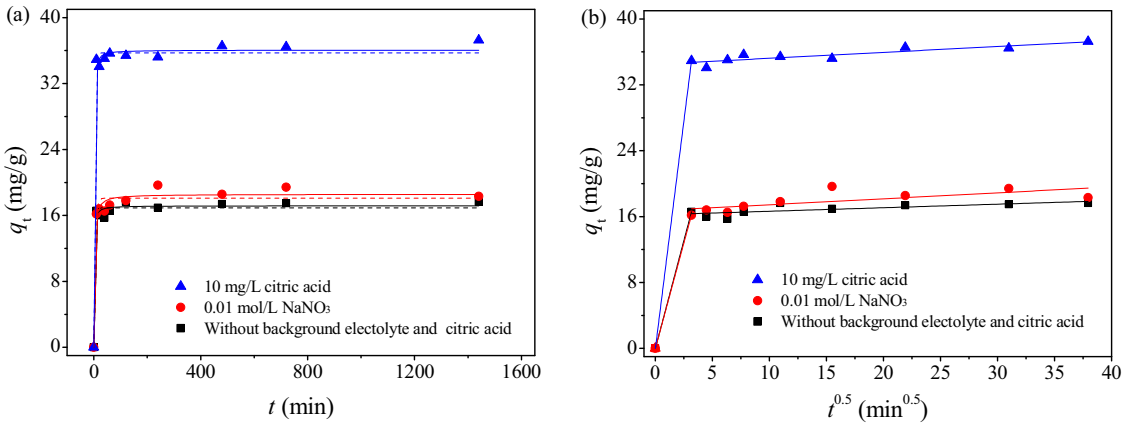

Fig. 6 – (a) Effects of 0.01 mol/L $NaNO_3$ and 10 mg/L citric acid on the time profiles of Cu(II) adsorption onto MGO/β-CD (The dash line and the solid line are pseudo-first-order and pseudo-second-order adsorption kinetics simulation, respectively.); (b) Intraparticle diffusion kinetics: $C_{0(Cu)}$ = 10 mg/L, *m*/V = 0.14 g/L, T = 30 °C, pH = 5.50 ± 0.02.

Table 1 – Kinetic parameters for adsorption of Cu(II) onto MGO/β-CD.

Groups	Pseudo-first-order			Pseudo-second-order			
	$k_1 \times 10$ (1/min)	$q_{e,1}$ (mg/g)	R^2	$k_2 \times 10^2$ (g/mg min)	$q_{e,2}$ (mg/g)	h (mg/g min)	R^2
Without BE and CA[a]	3.75	16.93	0.983	7.65	17.17	22.55	0.988
0.01 M $NaNO_3$	2.11	18.10	0.967	2.80	18.57	9.66	0.981
10 mg/L citric acid	3.70	35.71	0.993	4.98	36.06	64.76	0.995

[a] BE, background electrolyte; CA, citric acid.

are the adsorption capacity calculated by pseudo-first-order, pseudo-second-order models, respectively; k_1 (1/min) and k_2 (g/mg min) are the pseudo-first-order and pseudo-second-order adsorption rate constants, respectively. The initial adsorption rate h (mg/g min) can be calculated using the following equation (Djeribi and Hamdaoui, 2008):

$$h = k_2 q_{e,2}^2 \tag{4}$$

The non-linearized form of the pseudo-first-order and pseudo-second-order models is given in Fig. 6a, and the fitting results obtained from the two models are summarized in Table 1. It can be seen that the R^2 values of pseudo-second-order model (0.988, 0.981, and 0.995) were higher than those of pseudo-first-order model (0.983, 0.967, and 0.993). Moreover, the calculated q_e values of the pseudo-second-order model agreed with the experimental data better than those of the pseudo-first-order model. These indicated that the Cu(II) uptake processes followed the second-order type kinetic reaction, and because of the existence of the functional groups on the MGO/β-CD, the processes could be controlled by the chemical reaction (Song et al., 2013; Unlu and Ersoz, 2006). Similar results were observed in the adsorption of Hg(II) onto mercapto-grafted rice straw (Song et al., 2013). From Table 1, the initial adsorption rate h was the lowest in 0.01 M $NaNO_3$ solution (9.66 mg/g min) and was the highest in the system with the presence of 10 mg/L citric acid (64.76 mg/g min). This phenomenon may be attributed to the following: (1) the $NaNO_3$ in the solution could interact with the Cu(II) ions and the adsorbent, and this process was slow, which affected the initial adsorption process slightly; (2) when the citric acid was added to the adsorption system, it could be adsorbed by the MGO/β-CD immediately, and the *carboxyl groups of the* adsorbed citric acid had high affinity for Cu(II) ions, thereby improving the initial adsorption rate.

The pseudo-first-order and pseudo-second-order kinetic models have been used successfully to predict the possible adsorption behavior of Cu(II) ions onto MGO/β-CD, but these models did not reflect the Cu(II) ions transportation from the solution phase to the surface of the MGO/β-CD (Song et al., 2013). The four consecutive steps in the adsorption of a adsorbate by a adsorbent are: (1) transfer from the solution to the boundary film surrounding the adsorbent (bulk diffusion), (2) diffusion from the film to the external surface of the adsorbent (film diffusion), (3) diffusion in the internal structure of the adsorbent (intraparticle diffusion), and (4) adsorption on the internal surface of the adsorbent (Djeribi and Hamdaoui, 2008). The first and fourth steps are often assumed to be extremely rapid and can be ignored. Therefore, film diffusion and intraparticle diffusion are the possible rate-controlling steps (Cheung et al., 2007). In order to investigate the actual rate-controlling step involved in the adsorption processes of Cu(II) ions onto MGO/β-CD, the kinetic data were analyzed by applying the intraparticle diffusion model, which can be described as follows (Zhang et al., 2012):

$$q_t = k_p t^{0.5} + C \tag{5}$$

where k_p is the intraparticle diffusion model rate constant, and C is a constant related to the thickness of the boundary layer. Piecewise linear regression of the data shows that the plots (Fig. 6b) had two distinct regions. The first linear portion represented external mass transfer, and the second linear portion indicated the adsorption–desorption equilibrium, which suggested that intraparticle diffusion was not a rate-limiting step. The β-CD grafted on the MGO surface and the groups of the GO mainly existed on the surfaces of the adsorbent, therefore, the Cu(II) ions adsorption mostly occurred on the external surfaces of the MGO/β-CD. The intraparticle diffusion plots suggest that the Cu(II) diffusion in the boundary film (film diffusion) controls the adsorption rate.

3.6. *Adsorption isotherms*

The adsorption isotherm indicates the distribution relationship of the adsorbed heavy metal ions between the liquid phase and the solid phase when the adsorption process reaches equilibrium state (Liu et al., 2013). The Langmuir model assumes that a monomolecular layer is formed when adsorption takes place without any interaction between the adsorbed molecules (Aksu, 2002). The Freundlich isotherm model is applicable to both monolayer adsorption (chemisorption) and multilayer adsorption (physisorption) and is based on the assumption that the adsorbate is adsorbed onto the heterogeneous surface of an adsorbent (Yang, 1998). The Temkin isotherm is based on the heat of adsorption of the ions due to the adsorbate and adsorbent interactions (Boudrahem et al., 2011). The Langmuir, Freundlich, and Temkin models were applied to simulate the adsorption isotherms, and non-linearized form of these models can be described by the following equations:

$$\text{Langmuir}: \quad q_e = \frac{q_{\max} K_L C_e}{1 + K_L C_e} \tag{6}$$

$$\text{Freundlich}: \quad q_e = K_F C_e^{1/n} \tag{7}$$

$$\text{Temkin}: \quad q_e = \frac{RT}{b_T} \ln(a_T C_e) \tag{8}$$

where q_e (mg/g) is the amount of Cu(II) ions adsorbed on MGO/β-CD; $q_{\max}$ (mg/g) is the maximum amount of Cu(II) ions adsorbed per unit weight of MGO/β-CD to form a complete monolayer coverage on the surface. K_L (L/mg) is the Langmuir constant related to the affinity of the binding sites; C_e (mg/L) is the equilibrium concentration; K_F is the Freundlich constant related to adsorption capacity and n is the heterogeneity

Table 2 – The isotherm parameters for Cu(II) adsorption onto MGO/β-CD.

Models	Parameters	Groups		
		Without BE and CA[a]	0.01 M $NaNO_3$	10 mg/L citric acid
Langmuir isotherm				
	q_{max} (mg/g)	30.98	37.32	48.67
	K_L (L/mg)	0.190	0.253	2.249
	R^2	0.842	0.878	0.436
Freundlich isotherm				
	n	4.31	4.98	7.84
	K_F	10.97	15.35	30.37
	R^2	0.979	0.941	0.931
Temkin isotherm				
	a_T (L/g)	4.69	8.63	518.95
	b_T (KJ/mol)	0.500	0.450	0.513
	R^2	0.957	0.948	0.875

[a] BE, background electrolyte; CA, citric acid.

factor; R (8.314×10^{-3} kJ/mol K) is the gas constant and T (K) is the absolute temperature; a_T (L/g) is the equilibrium binding constant corresponding to the maximum binding energy; and b_T (kJ/mol) is the Temkin constant related to the heat of adsorption.

Isotherm experiments were conducted at different initial Cu(II) concentration (5, 10, 20, 40, 60, 80, and 100 mg/L) at pH 5.5 for 24 h, and the effects of 0.01 mol/L $NaNO_3$ and 10 mg/L citric acid on the adsorption isotherm were also investigated. The Langmuir and Freundlich adsorption isotherms obtained using the non-linearized method are shown in Fig. 7, and the calculated results of the isotherm constants are listed in Table 2. It is found that the Freundlich model could fit the experimental data better than the Langmuir model under different conditions. Wang and Chu (2011) also reported that Freundlich adsorption model better explained the adsorption of Rhodamine B (RhB) on silica fume (SF) and coal fly ash (CFA). The better fitting of the Freundlich isotherm model may be attributed to the heterogeneous distribution of adsorption active sites on MGO/β-CD surfaces (Gong et al., 2011; Ramesh et al., 2007). The Freundlich constant K_F indicates the adsorption capacity of the adsorbent. From Table 2, the value of K_F for Cu(II) adsorption onto MGO/β-CD in the adsorption system without $NaNO_3$ and citric acid addition was 10.97. While

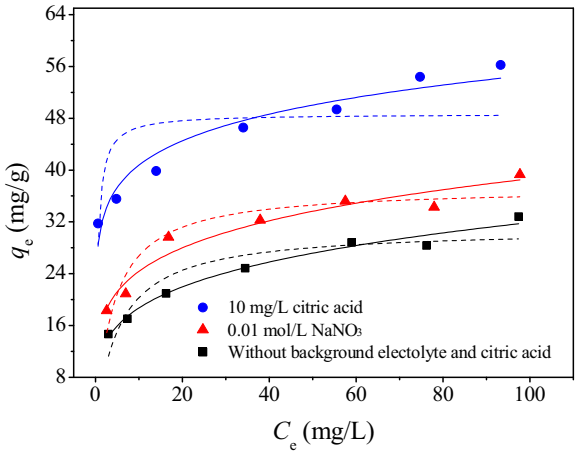

Fig. 7 – Effects of 0.01 mol/L $NaNO_3$ and 10 mg/L citric acid on the Langmuir (dash lines) and Freundlich (solid lines) adsorption isotherms for Cu(II) adsorption onto MGO/β-CD: m/V = 0.14 g/L, T = 30 °C, t = 24 h, pH = 5.50 ± 0.02.

in the systems with the presence of 0.01 mol/L $NaNO_3$ and 10 mg/L citric acid, the K_F values were 15.35 and 30.37, respectively. This indicated that the $NaNO_3$ and citric acid in the system could improve the adsorption capacity of MGO/β-CD for Cu(II). The Freundlich constant n is also an indication of the favorability of adsorption (Wang and Chu, 2011). Generally, n values between 1 and 10 represent beneficial adsorption based on mathematical calculations (Treybal, 1980). All the n values (Table 2) in this study were within the beneficial adsorption range, which indicates that MGO/β-CD can be used as an effective adsorbent.

As presented in Table 2, the adsorption data of Cu(II) ions on MGO/β-CD in the system without $NaNO_3$ and citric acid and in the system with addition of 0.01 mol/L $NaNO_3$ could be well fitted by Temkin isotherm model with high correlation coefficient values of 0.957 and 0.948, respectively. However, the Temkin model could not describe the adsorption data in the presence of 10 mg/L citric acid. We can also find that the value of the Temkin constant b_T in the presence of 0.01 mol/L $NaNO_3$ (0.450 kJ/mol) was lower than that in the absence of $NaNO_3$ and citric acid (0.500 kJ/mol), which suggested that the presence of $NaNO_3$ could enhance slightly the Cu(II) adsorption (Song et al., 2013). This is probably due to the reduction of the electrostatic repulsion between the Cu(II) and the MGO/β-CD by the $NaNO_3$. Besides, the higher value of a_T (8.63 L/g) for the system with presence of $NaNO_3$ indicates the good adsorption potential of the adsorbent in this solution (Babaeivelni and Khodadoust, 2013).

4. Conclusions

The analysis results of FESEM, TEM, TG–DSC, FT-IR, and zeta potential indicated that the MGO/β-CD composite was successfully prepared. MGO/β-CD shows excellent adsorption capacity for Cu(II) ions, and the adsorption process can be affected by the experimental conditions. High pH value is preferred for Cu(II) adsorption on the MGO/β-CD due to the increase in the negative surface charge of the adsorbent and the formation of precipitation. The introduction of β-CD to the MGO surface could increase efficiency of Cu(II) adsorption. The Cu(II) adsorption is dependent on ionic strength at low pH and is independent of ionic strength at high pH values. The presences of 0.01 mol/L $LiNO_3$, $NaNO_3$, KNO_3, NaCl, and $NaClO_4$ in the solution enhance the Cu(II) adsorption slightly, and different background electrolyte cations (Li^+, Na^+, and

K^+) have similar effects on the Cu(II) adsorption, while the background electrolyte anions of Cl^-, ClO_4^-, and NO_3^- have different influences on the Cu(II) removal. The presence of *citric acid* enhances the *Cu(II) adsorption* at various pH values. The Cu(II) adsorption processes can reach their equilibrium state within 10–30 min. The adsorption kinetics and isotherm can be affected by the presence of $NaNO_3$ and citric acid, and they can be well described by the pseudo-second-order kinetic model and the Freundlich isotherm, respectively. The rate controlling mechanism study revealed that the Cu(II) diffusion in the boundary film controls the adsorption rate. What's more, the adsorption data in the system without $NaNO_3$ and citric acid and the system with presence of $NaNO_3$ can be well fitted by Temkin isotherm model.

Acknowledgments

The authors would like to thank the financial support from the National Natural Science Foundation of China (Grant No. 41271332), the Natural Science Foundation of Hunan province, China (Grant No. 11JJ2031), the Science and Technology Planning Project of Hunan Province, China (Grant No. 2012SK2021), and the Hunan Provincial Innovation Foundation For Postgraduate (Grant No. CX2012B138).

References

Aksu, Z., 2002. Determination of the equilibrium, kinetic and thermodynamic parameters of the batch biosorption of nickel(II) ions onto *Chlorella vulgaris*. Process Biochem. 38, 89–99.

Babaeivelni, K., Khodadoust, A.P., 2013. Adsorption of fluoride onto crystalline titanium dioxide: effect of pH, ionic strength, and co-existing ions. J. Colloid Interface Sci. 394, 419–427.

Badruddoza, A.Z., Shawon, Z.B., Tay, W.J., Hidajat, K., Uddin, M.S., 2013. Fe_3O_4/cyclodextrin polymer nanocomposites for selective heavy metals removal from industrial wastewater. Carbohydr. Polym. 91, 322–332.

Boudrahem, F., Aissani-Benissad, F., Soualah, A., 2011. Adsorption of lead(II) from aqueous solution by using leaves of date trees as an adsorbent. J. Chem. Eng. Data 56, 1804–1812.

Cai, W., Tan, L., Yu, J., Jaroniec, M., Liu, X., Cheng, B., Verpoort, F., 2014. Synthesis of amino-functionalized mesoporous alumina with enhanced affinity towards Cr(VI) and CO_2. Chem. Eng. J. 239, 207–215.

Chen, C.Y., Chen, C.C., Chung, Y.C., 2007. Removal of phthalate esters by alpha-cyclodextrin-linked chitosan bead. Bioresour. Technol. 98, 2578–2583.

Chen, Z., Ma, W., Han, M., 2008. Biosorption of nickel and copper onto treated alga (*Undaria pinnatifida*): application of isotherm and kinetic models. J. Hazard. Mater. 155, 327–333.

Cheung, W.H., Szeto, Y.S., McKay, G., 2007. Intraparticle diffusion processes during acid dye adsorption onto chitosan. Bioresour. Technol. 98, 2897–2904.

Da'na, E., Sayari, A., 2013. Modeling adsorption of copper on amine-functionalized SBA-15: predicting breakthrough curves. J. Environ. Eng. 139, 95–103.

Djeribi, R., Hamdaoui, O., 2008. Sorption of copper(II) from aqueous solutions by cedar sawdust and crushed brick. Desalination 225, 95–112.

Donia, A.M., Atia, A.A., Yousif, S.S., 2013. Efficient adsorption of Cu(II) and Hg(II) from their aqueous solutions using amine functionalized cellulose. J. Dispers. Sci. Technol. 34, 1230–1239.

El-Bayaa, A.A., Badawy, N.A., AlKhalik, E.A., 2009. Effect of ionic strength on the adsorption of copper and chromium ions by vermiculite pure clay mineral. J. Hazard. Mater. 170, 1204–1209.

Fan, L., Luo, C., Sun, M., Qiu, H., 2012. Synthesis of graphene oxide decorated with magnetic cyclodextrin for fast chromium removal. J. Mater. Chem. 22, 24577.

Goldberg, S., 2005. Inconsistency in the triple layer model description of ionic strength dependent boron adsorption. J. Colloid Interface Sci. 285, 509–517.

Gong, J., Liu, T., Wang, X., Hu, X., Zhang, L., 2011. Efficient removal of heavy metal ions from aqueous systems with the assembly of anisotropic layered double hydroxide nanocrystals@carbon nanosphere. Environ. Sci. Technol. 45, 6181–6187.

Guo, Y.J., Guo, S.J., Ren, J.T., Zhai, Y.M., Dong, S.J., Wang, E.K., 2010. Cyclodextrin functionalized graphene nanosheets with high supramolecular recognition capability: synthesis and host–guest inclusion for enhanced electrochemical performance. ACS Nano 4, 5512.

Ho, Y.S., Wase, D.A.J., Forster, C.F., 1996. Kinetic studies of competitive heavy metal adsorption by sphagnum moss peat. Environ. Technol. 17, 71–77.

Hu, X.J., Liu, Y.G., Wang, H., Chen, A.W., Zeng, G.M., Liu, S.M., Guo, Y.M., Hu, X., Li, T.T., Wang, Y.Q., Zhou, L., Liu, S.H., 2013. Removal of Cu(II) ions from aqueous solution using sulfonated magnetic graphene oxide composite. Sep. Purif. Technol. 108, 189–195.

Hu, X.J., Wang, J.S., Liu, Y.G., Li, X., Zeng, G.M., Bao, Z.L., Zeng, X.X., Chen, A.W., Long, F., 2011. Adsorption of chromium(VI) by ethylenediamine-modified cross-linked magnetic chitosan resin: isotherms, kinetics and thermodynamics. J. Hazard. Mater. 185, 306–314.

Jiang, J., Xu, R.-k., Li, S.-z., 2010. Effect of ionic strength and mechanism of Cu(II) adsorption by goethite and γ-Al_2O_3. J. Chem. Eng. Data 55, 5547–5552.

Khaled, A., El Nemr, A., EI-Sikaily, A., Abdelwahab, A., 2009. Treatment of artificial textile dye effluent containing Direct Yellow 12 by orange peel carbon. Desalination 238, 210–232.

Konkena, B., Vasudevan, S., 2012. Covalently linked, water-dispersible, cyclodextrin: reduced-graphene oxide sheets. Langmuir 28, 12432–12437.

Kozlowski, C., Girek, T., Walkowiak, W., Koziol, J., 2005. Application of hydrophobic β-cyclodextrin polymer in separation of metal ions by plasticized membranes. Sep. Purif. Technol. 46, 136–144.

Lam, K.F., Chen, X., McKay, G., Yeung, K.L., 2008. Anion effect on Cu^{2+} adsorption on NH_2-MCM-41. Ind. Eng. Chem. Res. 47, 9376–9383.

Li, J., Zhang, S.W., Chen, C.L., Zhao, G.X., Yang, X., Li, J.X., Wang, X.K., 2012. Removal of Cu(II) and fulvic acid by graphene oxide nanosheets decorated with Fe_3O_4 nanoparticles. ACS Appl. Mater. Interfaces 4, 4991–5000.

Liu, M.C., Chen, C.L., Hu, J., Wu, X.L., Wang, X.K., 2011. Synthesis of magnetite/graphene oxide composite and application for cobalt(II) removal. J. Phys. Chem. C 115, 25234–25240.

Liu, T., Duan, X., Duan, G., Wu, W., Ying, Y., Zhang, Y.H., 2013. Adsorption of UO_2^{2+} on poly(N,N-diethylacrylamide-co-acrylic acid): effects of pH, ionic strength, initial uranyl concentration, and temperature. J. Radioanal. Nucl. Chem. 298, 571–580.

Manzoor, Q., Nadeem, R., Iqbal, M., Saeed, R., Ansari, T.M., 2013. Organic acids pretreatment effect on Rosa bourbonia phyto-biomass for removal of Pb(II) and Cu(II) from aqueous media. Bioresour. Technol. 132, 446–452.

Mohan, D., Pittman, C.U., 2006. Activated carbons and low cost adsorbents for remediation of tri- and hexavalent chromium from water. J. Hazard. Mater. 137, 762–811.

Nomanbhay, S.M., Palanisamy, K., 2005. Removal of heavy metal from industrial wastewater using chitosan coated oil palm shell charcoal. Electron. J. Biotechnol. 8, 43–53.

Ohashi, H., Hiraoka, Y., Yamaguchi, T., 2006. An autonomous phase transition-complexation/decomplexation polymer system with a molecular recognition property. Macromolecules 39, 2614–2620.

Pan, N., Deng, J., Guan, D., Jin, Y., Xia, C., 2013. Adsorption characteristics of Th(IV) ions on reduced graphene oxide from aqueous solutions. Appl. Surf. Sci. 287, 478–483.

Parida, K., Mishra, K.G., Dash, S.K., 2012. Adsorption of copper(II) on NH_2-MCM-41 and its application for epoxidation of styrene. Ind. Eng. Chem. Res. 51, 2235–2246.

Ramesh, A., Hasegawa, H., Maki, T., Ueda, K., 2007. Adsorption of inorganic and organic arsenic from aqueous solutions by polymeric Al/Fe modified montmorillonite. Sep. Purif. Technol. 56, 90–100.

Saman, N., Johari, K., Mat, H., 2014. Adsorption characteristics of sulfur-functionalized silica microspheres with respect to the removal of Hg(II) from aqueous solutions. Ind. Eng. Chem. Res. 53, 1225–1233.

Song, S.-T., Saman, N., Johari, K., Mat, H., 2013. Removal of Hg(II) from aqueous solution by adsorption using raw and chemically modified rice straw as novel adsorbents. Ind. Eng. Chem. Res. 52, 13092–13101.

Szejtli, J., 1998. Introduction and general overview of cyclodextrin chemistry. Chem. Rev. 98, 1743–1754.

Tan, X., Wang, X., Chen, C., Sun, A., 2007. Effect of soil humic and fulvic acids, pH and ionic strength on Th(IV) sorption to TiO_2 nanoparticles. Appl. Radiat. Isot. 65, 375–381.

Tao, Z.Y., Chu, T.W., Li, W.J., Du, J.Z., Dai, X.X., Gu, Y.J., 2004. Cation adsorption of NpO^{2+}, $UO_2{}^{2+}$, Zn^{2+}, Sr^{2+}, Yb^{3+}, and Am^{3+} onto oxides of Al, Si, and Fe from aqueous solution: ionic strength effect. Colloids Surf., A 242, 39–45.

Treybal, R.E., 1980. Mass Transfer Operations. McGraw-Hill Higher Education, New York.

Unlu, N., Ersoz, M., 2006. Adsorption characteristics of heavy metal ions onto a low cost biopolymeric sorbent from aqueous solutions. J. Hazard. Mater. 136, 272–280.

Wang, Y.R., Chu, W., 2011. Adsorption and removal of a xanthene dye from aqueous solution using two solid wastes as adsorbents. Ind. Eng. Chem. Res. 50, 8734–8741.

Yang, C.-h., 1998. Statistical mechanical study on the Freundlich isotherm equation. J. Colloid Interface Sci. 208, 379–387.

Yang, J.K., Lee, S.M., Davis, A.P., 2006. Effect of background electrolytes and pH on the adsorption of Cu(II)/EDTA onto TiO_2. J. Colloid Interface Sci. 295, 14–20.

Yang, S.B., Hu, J., Chen, C.L., Shao, D.D., Wang, X.K., 2011. Mutual effects of Pb(II) and humic acid adsorption on multiwalled carbon nanotubes/polyacrylamide composites from aqueous solutions. Environ. Sci. Technol. 45, 3621–3627.

Yang, S.T., Sheng, G.D., Guo, Z.Q., Tan, X.L., Xu, J.Z., Wang, X.K., 2012. Investigation of radionuclide ^{63}Ni(II) sequestration mechanisms on mordenite by batch and EXAFS spectroscopy study. Sci. China Chem. 42, 844–855.

Yang, Y., Wang, J., Zhang, J., Liu, J., Yang, X., Zhao, H., 2009. Exfoliated graphite oxide decorated by PDMAEMA chains and polymer particles. Langmuir 25, 11808–11814.

Zhang, L., Jiang, X.Q., Xu, T.C., Yang, L.J., Zhang, Y.Y., Jin, H.J., 2012. Sorption characteristics and separation of rhenium ions from aqueous solutions using modified nano-Al_2O_3. Ind. Eng. Chem. Res. 51, 5577–5584.

Zhang, W., Zhou, C., Zhou, W., Lei, A., Zhang, Q., Wan, Q., Zou, B., 2011. Fast and considerable adsorption of methylene blue dye onto graphene oxide. Bull. Environ. Contam. Toxicol. 87, 86–90.

Zhao, G.X., Li, J.X., Ren, X.M., Chen, C.L., Wang, X.K., 2011. Few-layered graphene oxide nanosheets as superior sorbents for heavy metal ion pollution management. Environ. Sci. Technol. 45, 10454–10462.